2011 50th IEEE Conference on Decision and Control and
European Control Conference (CDC-ECC)
Orlando, FL, USA, December 12-15, 2011

Retrospective Cost Adaptive Control for a Ground Tethered Energy System

Matthew W. Isaacs*, Jesse B. Hoagg†, Islam I. Hussein‡, and David Olinger§

Abstract— **Ground tethered energy (GTE) systems are a promising technology for addressing the challenge of sustainable electric power production. This paper presents a GTE system that converts wind energy into electric energy by using a kite tethered to a spooling system. More specifically, this system converts the kinetic energy from the kite's motion into electric energy. In this paper, we introduce a dynamic model for the ground-tethered kite and present an adaptive controller that is effective for controlling the kite's motion. In particular, we present simulation results that demonstrate adaptive command following, where the kite system is able to harvest energy from the wind.**

I. Introduction

The combustion of fossil fuels is currently used to meet the majority of global energy needs. Sustainable methods for electric power production are needed to address future shortages of fossil fuels as well as climate change implications of burning fossil fuels. One potential sustainable energy resource is wind energy. The recent study [1] proposes that, by 2030, twenty percent of US power consumption should be met by wind power sources. Wind farms, consisting of hundreds of large wind turbines spaced relatively close together, can be used to capture available wind energy in high-wind areas. However, these large turbines require heavy towers, foundations, and huge blades, which have significant environmental impact, require large resource investments, and have long amortization periods. In addition, wind farms generate up to 300 times less power per area of land than power plants burning fossil fuels [2].

Ground tethered energy (GTE) systems have received less attention than wind turbines, but some investigations were conducted in the late 1970s and early 1980s [3]–[5] as well as more recently in [2], [6]–[10]. A GTE system consists of a lifting body (e.g., light-weight kite or rigid-wing glider) that flies at high altitudes (i.e., up to 1,000 meters) and is controlled by an automatic flight control system. A flexible tether is used to transmit the aerodynamic forces on the kite to a power conversion system on the ground. In some proposed schemes, the power conversion takes place on the lifting body by using turbines carried on the lifting body [4]. However, these systems have the disadvantage that a significant amount of power is required to lift the turbines. The focus of the present work is on tethered systems that use light-weight gliders (or kites) as the lifting body and where the power conversion is conducted on the ground.

As opposed to wind turbines, GTE systems can be cost-effective in low-wind-speed areas because:

- kites can fly at altitudes above those where wind turbines operate, which leads to higher available wind power densities;
- kites do not require expensive tower structures;
- kites can move at high velocities in cross-wind motions to increase electric power production.

Figure 1 diagrams a GTE system. The kite ascends during a power-generation phase, where tension is placed on the tether, which unrolls from a spool placed at the anchor point, and the spool turns a generator to create power. During a retraction phase, the tether tension is reduced (by decreasing the kite's angle of attack), and the tether is reeled in by a motor using only a portion of the power generated. The kite's motion can be controlled manipulating the kite's trailing edge, wingtips, or other control surfaces.

For a GTE system, adaptive control offers several potential benefits, including the ability to adapt to changing wind conditions and flight conditions. In addition, an adaptive control approach requires extracting limited model information from the GTE system as opposed to other control approaches, which could require more extensive model information.

In the present paper, we first derive the equations of motion for a GTE system. Next, we use an adaptive control algorithm (namely, the retrospective cost adaptive control (RCAC) algorithm, which is presented in [11], [12]) to control the pitch and roll angles of the ground-tethered kite. We simulate the ground-tethered kite with RCAC operating in feedback and force the kite's pitch and roll angles to follow sinusoidal command signals, which results in a power-generating flight trajectory.

RCAC is a discrete-time adaptive control technique for systems that are possibly nonminimum-phase, provided that the nonminimum-phase zeros are known [11]–[14]. RCAC's ability to control nonminimum-phase systems is important for application to the ground-tethered kite system because certain linearized transfer functions of the kite system have nonminimum-phase zeros (as discussed in Section IV). More specifically, the linearized roll-moment-to-roll-angle Markov parameters and the linearized pitch-moment-to-pitch-angle Markov parameters (which we estimate through numerical testing) suggest that these linearized transfer functions have nonminimum-phase zeros near -1 in the $\mathbf{z}$-domain.

*Graduate Student, Department of Mechanical Engineering, The University of Kentucky, Lexington, KY, 40506-0503, email: matthew.isaacs@uky.edu.

†Assistant Professor, Department of Mechanical Engineering, The University of Kentucky, Lexington, KY, 40506-0503, email: jhoagg@engr.uky.edu.

‡Assistant Professor, Department of Mechanical Engineering, Worcester Polytechnic Institute, Worcester, MA 01609, email: ihussein@wpi.edu.

§Associate Professor, Department of Mechanical Engineering, Worcester Polytechnic Institute, Worcester, MA 01609, email: olinger@wpi.edu.

978-1-61284-799-3/11/$26.00 ©2011 IEEE

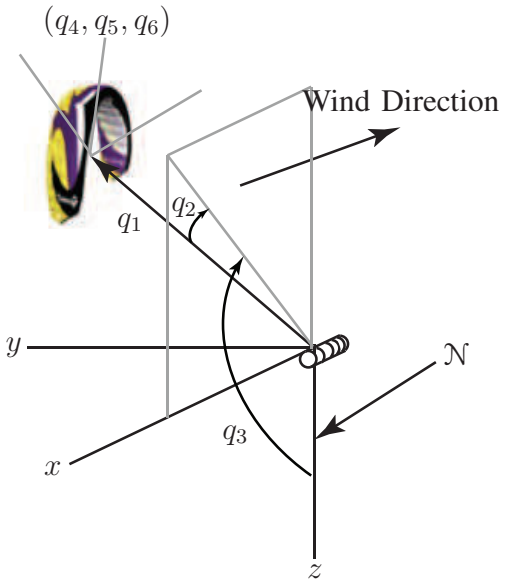

Fig. 1. Kite and tether system coordinates.

II. Ground-Tethered Kite Equations of Motion

A. Coordinate System and System Inertia Properties

The kite is modeled as a three-dimensional rigid body, tethered to a fixed point on the ground. The tether is assumed to be straight. The inertial space-fixed coordinate system $\mathcal{N}$ is attached to the ground, with its origin located at the point where the kite is anchored (see Figure 1). Hence, the system has a model similar to the inverted pendulum, except that the tether length q_1 is allowed to vary with time and thus is a configuration variable. The tether is hinged at the kite's center of mass, which has spherical coordinates (q_1, q_2, q_3). The kite's attitude is specified using the roll, pitch and yaw coordinates (q_4, q_5, q_6). Hence, we have a six dimensional configuration space with a twelve dimensional phase space. The kite has mass M and a principal moment of inertia matrix $\mathbf{J}$. The tether is assumed to have a uniform density per unit length ρ. Next, we describe the kinetic and potential energies that are used to derive the Lagrangian and the equations of motion.

B. Kinetic Energy

The system's kinetic energy is given by the sum of the kinetic energy of the tether and the kinetic energy of the kite. Consider a point located a distance of s along the tether from the origin. The position vector of that point is given by

$$\mathbf{r}(s) = (s\cos q_2 \sin q_3, s\sin q_2, s\cos q_2 \cos q_3),$$

and, therefore, the velocity of the point is given by

$$\begin{aligned}\dot{\mathbf{r}}(s) \;=\; & \big(\dot{q}_1 \cos q_2 \sin q_3 - s\dot{q}_2 \sin q_2 \sin q_3 \\ & + s\dot{q}_3 \cos q_2 \cos q_3, \\ & \dot{q}_1 \sin q_2 + s\dot{q}_2 \cos q_2, \\ & \dot{q}_1 \cos q_2 \cos q_3 - s\dot{q}_2 \sin q_2 \cos q_3 \\ & - s\dot{q}_3 \cos q_2 \sin q_3\big),\end{aligned}$$

where we assume that the tether is rigid (i.e, $\dot{s} = \dot{q}_1$). Hence, the kinetic energy for the tether is given by

$$\begin{aligned}K_t(\mathbf{q}, \dot{\mathbf{q}}) \;&=\; \frac{1}{2}\rho \int_0^{q_1} \dot{\mathbf{r}}(s)\cdot\dot{\mathbf{r}}(s)\mathrm{d}s \\ &=\; \frac{1}{6}\rho q_1 \left(3\dot{q}_1^2 + q_1^2\ \left(\dot{q}_2^2 + \dot{q}_3^2\cos^2 q_2\right)\right). \quad (1)\end{aligned}$$

The kinetic energy of the kite is the sum of its translational and rotational kinetic energies and is given by

$$\begin{aligned}K_k(\mathbf{q}, \dot{\mathbf{q}}) \;&=\; \frac{1}{2}M\dot{\mathbf{r}}(q_1)\cdot\dot{\mathbf{r}}(q_1) + \frac{1}{2}\boldsymbol{\Omega}\cdot\mathbf{J}\cdot\boldsymbol{\Omega} \\ &=\; \frac{1}{2}M\left(\dot{q}_1^2 + q_1^2\left(\dot{q}_2^2 + \dot{q}_3^2\cos^2 q_2\right)\right) \\ &\qquad + \frac{1}{2}\left(J_1\omega_1^2 + J_2\omega_2^2 + J_3\omega_3^2\right),\end{aligned}$$

where

$$\boldsymbol{\Omega} = \begin{bmatrix} 0 & -\omega_3 & \omega_2 \\ \omega_3 & 0 & -\omega_1 \\ -\omega_2 & \omega_1 & 0 \end{bmatrix}$$

is the angular velocity of the kite in the body frame, which we assume to be aligned with the principal axis frame. Let $\mathbf{R}$ denote the rotation matrix of the kite's principal axis with respect to $\mathcal{N}$. Then the angular velocity $\boldsymbol{\Omega}$ and the rotation matrix $\mathbf{R}$ are related via the rigid body kinematic equation $\dot{\mathbf{R}} = \mathbf{R}\boldsymbol{\Omega}$. Thus, the overall system kinetic energy is given by $K(\mathbf{q}, \dot{\mathbf{q}}) = K_t(\mathbf{q}, \dot{\mathbf{q}}) + K_k(\mathbf{q}, \dot{\mathbf{q}})$.

C. Potential Energy

Assuming that the kite has a uniform mass distribution, the overall system potential energy function is given by $V(\mathbf{q}) = \frac{1}{2}\rho g q_1^2 \cos q_2 \cos q_3 + Mgq_1 \cos q_2 \cos q_3$.

D. Lift and Drag

Let $\mathbf{F}_d(\mathbf{q})$ and $\mathbf{F}_l(\mathbf{q})$ denote the drag and lift forces acting on the kite. We note that $\mathbf{F}_d$ and $\mathbf{F}_l$ are functions of only (q_4, q_5, q_6), wind speed, and the kite geometry. The expressions for lift and drag on the kite are given in [6]. Note that [6] studies a three-dimensional kite model that treats the kite as a point mass at the end of the tether, as opposed to a full rigid body with its own lift and drag forces as we do in this paper. Specifically, we use linear aerodynamic and lifting-line wing theory to estimate the kite's lift and drag (for angles below the kite's stall angle). In addition, we calculate the kite's roll and pitch moments using pitch and roll angle linear perturbation techniques, which rely on the slope of the rolling moment coefficient versus roll angle as well as the slope of the pitching moment coefficient versus angle of attack. For more information, see for example [15]–[17].

E. System Lagrangian and Equations of Motion

The Lagrangian is given $L(\mathbf{q}, \dot{\mathbf{q}}) = K(\mathbf{q}, \dot{\mathbf{q}}) - V(\mathbf{q})$ and the equations of motion can be obtained from the Euler-Lagrange equations

$$\frac{\mathrm{d}}{\mathrm{d}t}\frac{\partial L}{\partial \dot{q}_i} - \frac{\partial L}{\partial q_i} = v_i + F_{di} + F_{li}, \quad (2)$$

where F_{di} and F_{li} are the drag and lift forces or moments acting in the i direction, and v_i is the component of the generalized control forces acting in the i direction.

The equations of motion that result from (2) are symbolically complex, and we omit them for the sake of brevity. However, the equations have been verified by showing that they reduce to the same form as those of known systems. For example, by setting $\rho = 0$, we obtained the standard equations for an aircraft [17]. By letting $\mathbf{J} = 0$ and q_1 be constant, we obtained the standard equations for an inverted pendulum. Finally, we have verified the equations (2) numerically by comparing their solutions to solutions obtained from the equations of motion derived using non-Lagrangian techniques (namely, Newton's Second Law, which results in higher order constrained differential equations).

III. Retrospective Cost Adaptive Control

In this section, we review the recursive-least-squares-based retrospective cost adaptive control (RCAC) algorithm presented in [11]. The stability analysis for the RCAC algorithm is provided in [12]. In this section, we also highlight the model information required by the adaptive controller. The process for estimating this information for the ground-tethered kite is discussed in Section IV.

First, consider the multi-input, multi-output linear discrete-time system

$$y(k) = \sum_{i=1}^{n} -\alpha_i y(k-i) + \sum_{i=d}^{n} \beta_i u(k-i) + \sum_{i=0}^{n} \gamma_i w(k-i), \tag{3}$$

where $\alpha_1, \ldots, \alpha_n \in \mathbb{R}$, $\beta_d, \ldots, \beta_n \in \mathbb{R}^{l\times l}$, $\gamma_0, \ldots, \gamma_n \in \mathbb{R}^{l\times l_w}$, $y(k)$ is the output, $u(k)$ is the control, $w(k)$ is an unknown bounded exogenous disturbance, and the relative degree is $d > 0$.

For this point forward, let $\mathbf{q}$ and $\mathbf{q}^{-1}$ denote the forward-shift and backward-shift operators, respectively. Next, define $\beta(\mathbf{q}) \triangleq \beta_d \mathbf{q}^{n-d} + \beta_{d+1}\mathbf{q}^{n-d-1} + \cdots + \beta_{n-1}\mathbf{q} + \beta_n$ and consider the polynomial matrix factorization $\beta(\mathbf{q}) = \beta_{\mathrm{u}}(\mathbf{q})\beta_{\mathrm{s}}(\mathbf{q})$, where $\beta_{\mathrm{u}}(\mathbf{q})$ is an $l\times l$ polynomial matrix; $\beta_{\mathrm{s}}(\mathbf{q})$ is a monic $l\times l$ polynomial matrix; and if $\lambda \in \mathbb{C}$, $|\lambda| \geq 1$, and $\det \beta(\lambda) = 0$, then $\det \beta_{\mathrm{u}}(\lambda) = 0$ and $\det \beta_{\mathrm{s}}(\lambda) \neq 0$. We assume that the matrix polynomial $\beta_{\mathrm{u}}(\mathbf{q})$ is known, which implies that the nonminimum-phase zeros from u to y are known. The matrix polynomial $\beta_{\mathrm{u}}(\mathbf{q})$ is the only model information required by the adaptive controller. Section IV discusses a technique for estimating this information for the linearized GTE system.

Next, let $r(k) \in \mathbb{R}^l$ be an exogenous command signal that is generated by an unforced Lyapunov stable linear system. Define the tracking error $z(k) \triangleq y(k) - r(k)$. Our goal is to drive $z(k)$ to zero in the presence of the unknown disturbance $w(k)$. To achieve this goal, we use a time-series controller of order n_{c}, which is given by

$$u(k) = \sum_{i=1}^{n_{\mathrm{c}}} M_i(k)u(k-i) + \sum_{i=1}^{n_{\mathrm{c}}} L_i(k)z(k-i), \tag{4}$$

where, for all $i = 1, \ldots, n_{\mathrm{c}}$, $L_i : \mathbb{N} \to \mathbb{R}^{l\times l}$ and $M_i : \mathbb{N} \to \mathbb{R}^{l\times l}$ are determined by the adaptive control law presented below. The control (4) can be expressed as

$$u(k) = \Psi^{\mathrm{T}}(k)\Theta(k), \tag{5}$$

where

$$\Theta(k) \triangleq \mathrm{vec}\left[\begin{array}{cccccc} L_1(k) & \cdots & L_{n_{\mathrm{c}}}(k) & M_1(k) & \cdots & M_{n_{\mathrm{c}}}(k) \end{array}\right],$$
$$\Psi(k) \triangleq \phi(k) \otimes I_l \in \mathbb{R}^{2n_{\mathrm{c}}l^2\times l},$$
$$\phi(k) \triangleq \left[\begin{array}{ccc} z^{\mathrm{T}}(k-1) & \cdots & z^{\mathrm{T}}(k-n_{\mathrm{c}}) \\ u^{\mathrm{T}}(k-1) & \cdots & u^{\mathrm{T}}(k-n_{\mathrm{c}}) \end{array}\right]^{\mathrm{T}} \in \mathbb{R}^{2n_{\mathrm{c}}l},$$

and $\otimes$ is the Kronecker product.

Next, let $\alpha_*(\mathbf{q})$ be an asymptotically stable monic polynomial with degree $n_{\mathrm{c}} + n_{\mathrm{u}} + d$, where n_{u} is the degree of $\beta_{\mathrm{u}}(\mathbf{q})$. The polynomial $\alpha_*(\mathbf{q})$ is the characteristic polynomial associated with the target closed-loop dynamics of the adaptive system. Finally, define the filtered tracking error $z_{\mathrm{f}}(k) \triangleq \bar{\alpha}_*(\mathbf{q}^{-1})z(k)$, where $\bar{\alpha}_*(\mathbf{q}^{-1}) \triangleq \mathbf{q}^{-n_{\mathrm{c}}-n_{\mathrm{u}}-d}\alpha_*(\mathbf{q})$.

Now, let $\hat{\Theta} \in \mathbb{R}^{2n_{\mathrm{c}}l^2}$ be an optimization variable, and define the retrospective performance

$$\hat{z}(\hat{\Theta}, k) \triangleq z_{\mathrm{f}}(k) + \Phi^{\mathrm{T}}(k)\hat{\Theta} - \bar{\beta}_{\mathrm{u}}(\mathbf{q}^{-1})u(k),$$

where

$$\Phi(k) \triangleq \left[\bar{\beta}_{\mathrm{u}}(\mathbf{q}^{-1})\Psi^{\mathrm{T}}(k)\right]^{\mathrm{T}},$$

and $\bar{\beta}_{\mathrm{u}}(\mathbf{q}^{-1}) \triangleq \mathbf{q}^{-n_{\mathrm{u}}-d}\beta_{\mathrm{u}}(\mathbf{q})$. Furthermore, define the cumulative retrospective cost function

$$J(\hat{\Theta}, k) \triangleq \sum_{i=0}^{k} \lambda^{k-i}\hat{z}^{\mathrm{T}}(\hat{\Theta}, i)\hat{z}(\hat{\Theta}, i) + \lambda^k[\hat{\Theta} - \Theta(0)]^{\mathrm{T}}R[\hat{\Theta} - \Theta(0)],$$

where $R \in \mathbb{R}^{2n_{\mathrm{c}}l^2\times 2n_{\mathrm{c}}l^2}$ is positive definite, $\lambda \in (0, 1]$ is a forgetting factor, and $\Theta(0) \in \mathbb{R}^{2n_{\mathrm{c}}l^2}$.

The cumulative retrospective cost function $J(\hat{\Theta}, k)$ is minimized by a recursive-least-squares (RLS) algorithm with a forgetting factor. For each $k \geq 0$, $J(\hat{\Theta}, k)$ is minimized by

$$\Theta(k+1) = \Theta(k) - P(k)\Phi(k)\Omega(k)^{-1}z_{\mathrm{f,r}}(k), \tag{6}$$
$$P(k+1) = \frac{1}{\lambda}P(k) - \frac{1}{\lambda}P(k)\Phi(k)\Omega(k)^{-1}\Phi^{\mathrm{T}}(k)P(k), \tag{7}$$

where $\Omega(k) \triangleq \lambda I + \Phi^{\mathrm{T}}(k)P(k)\Phi(k)$, $P(0) = R^{-1}$, and $z_{\mathrm{f,r}}(k) \triangleq \hat{z}(\Theta(k), k)$. In summary, the RLS-based RCAC is given by (5), (6), and (7). The controller architecture is shown in Figure 2.

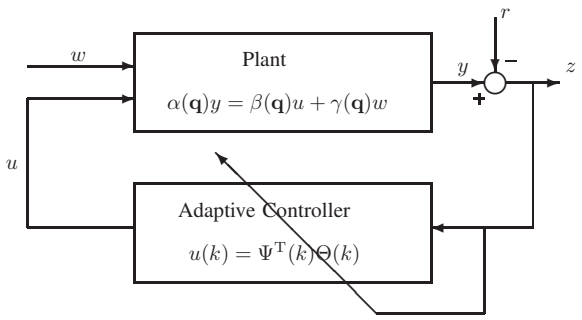

Fig. 2. Schematic diagram of the RCAC algorithm given by (5)-(7).

IV. Implementation of RCAC and Estimating the Required Model Information

In this section, we describe the implementation of the RCAC algorithm on the ground-tethered kite. The ground-tethered kite, given by (2), is a continuous-time dynamical system, and RCAC is a discrete-time algorithm. Thus, we implement RCAC with a zero-order hold on the inputs and a sampling time of $T_{\mathrm{s}} = 0.05$ seconds (which is sufficiently fast for the speed of the system dynamics). Note that RCAC, presented in Section III, is based on a linear model of the plant; however, we stress that in this paper we use this technique to control the full nonlinear ground-tethered kite model.

We assume that the ground-tethered kite has two control inputs, namely, a rolling moment $u_{\mathrm{r}}(k)$ and a pitching moment $u_{\mathrm{p}}(k)$. Thus, it follows from (2) that the generalized control force v_4 is the zero-order hold of $u_{\mathrm{r}}(k)$ and v_5 is the zero-order hold of $u_{\mathrm{p}}(k)$. Furthermore, there are no other control forces, that is, v_1, v_2, v_3, and v_6 from (2) are identically zero. Next, we assume that there are two measurements available for feedback, namely, the roll angle $y_{\mathrm{r}}(k)$ and the pitch angle $y_{\mathrm{p}}(k)$. Note that $y_{\mathrm{r}}(k)$ is the sampled-data signal obtained from q_4 and $y_{\mathrm{p}}(k)$ is the sampled-data signal obtained from q_5.

Our objective is to force $y_{\mathrm{p}}(k)$ and $y_{\mathrm{r}}(k)$ to follow the external commands $r_{\mathrm{p}}(k)$ and $r_{\mathrm{r}}(k)$, respectively. Thus, we define the pitch angle tracking error $z_{\mathrm{p}}(k) \triangleq y_{\mathrm{p}}(k) - r_{\mathrm{p}}(k)$ and the roll angle tracking error $z_{\mathrm{r}}(k) \triangleq y_{\mathrm{r}}(k) - r_{\mathrm{r}}(k)$.

We implement two separate RCAC control loops. The first control loop is a single-input, single-output loop that controls the ground-tethered kite's behavior from pitching moment $u_{\mathrm{p}}(k)$ to pitch angle $y_{\mathrm{p}}(k)$. The second control loop is a single-input, single-output loop that controls the ground-tethered kite's behavior from rolling moment $u_{\mathrm{r}}(k)$ to roll angle $y_{\mathrm{r}}(k)$. Thus, from a control design perspective, we ignore the pitching-moment-to-roll-angle and rolling-moment-to-pitch-angle effects (although these effects do exist within the nonlinear ground-tethered kite model). This design choice is supported by numerical tests, which suggest that the pitching-moment-to-pitch-angle dynamics are weakly coupled to the rolling-moment-to-roll-angle dynamics. Figure 3 is a schematic diagram, which shows the two-control-loop implementation of RCAC. For the remainder of this paper, we use the controller notation from Section III and add the subscript p to denote the pitching-moment-to-pitch-angle dynamics and control loop, or the subscript r to denote the rolling-moment-to-roll-angle dynamics and control loop.

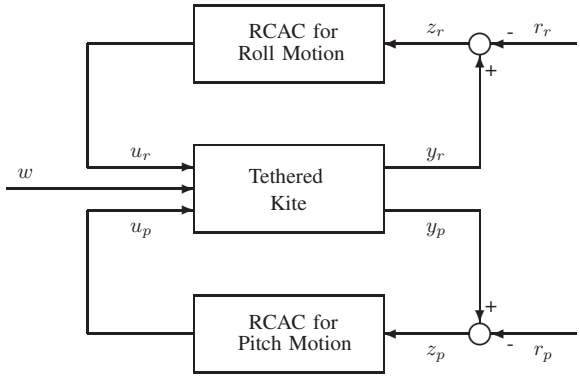

Fig. 3. Schematic diagram of the two-control-loop RCAC.

In order to implement the two RCAC loops, we require estimates of $\beta_{\mathrm{u,p}}(\mathbf{q})$ and $\beta_{\mathrm{u,r}}(\mathbf{q})$, which characterize the nonminimum-phase zeros of the linearized GTE system. However, the polynomials $\beta_{\mathrm{u,p}}(\mathbf{q})$ and $\beta_{\mathrm{u,r}}(\mathbf{q})$ can be estimated from a finite number of Markov parameters of the linearized tethered kite system. For example, let $G_{\mathrm{p}}(\mathbf{z})$ denote the transfer function of the linearized tethered kite from $u_{\mathrm{p}}(k)$ to $y_{\mathrm{p}}(k)$. The Laurent series expansion of $G_{\mathrm{p}}(\mathbf{z})$ about $\mathbf{z} = \infty$ is $G_p(\mathbf{z}) = \sum_{i=1}^{\infty} \mathbf{z}^{-i} H_{\mathrm{p},i}$, where $H_{\mathrm{p},1}, H_{\mathrm{p},2}, \ldots$ are the Markov parameters of the linearized system from $u_{\mathrm{p}}(k)$ to $y_{\mathrm{p}}(k)$. Truncating the Laurent series expansion after $\mu+1$ terms yields the truncated Laurent series expansion of $G_{\mathrm{p}}(\mathbf{z})$ about $\mathbf{z} = \infty$, which is given by $\bar{G}_p(\mathbf{z}) = \sum_{i=1}^{\mu+1} \mathbf{z}^{-i} H_{\mathrm{p},i}$. Next, since $G_{\mathrm{p}}(\mathbf{z})$ is an asymptotically stable single-input, single-output transfer function, it follows that a subset of the roots of $H_{\mathrm{p}}(\mathbf{z}) \triangleq H_{\mathrm{p},1}\mathbf{z}^{\mu} + H_{\mathrm{p},2}\mathbf{z}^{\mu-1} + \cdots + H_{\mathrm{p},\mu}\mathbf{z} + H_{\mathrm{p},\mu+1}$ can be shown to approximate the nonminimum-phase zeros of $G_{\mathrm{p}}(\mathbf{z})$. Thus, $\beta_{\mathrm{u,p}}(\mathbf{q})$ and $\beta_{\mathrm{u,r}}(\mathbf{q})$ can be estimated from a finite number of Markov parameters.

We use the observer/Kalman-filter identification (OKID) algorithm (see [18]) to estimate the pitching-moment-to-pitch-angle Markov parameters and rolling-moment-to-roll-angle Markov parameters of the linearized tethered kite system. In particular, the tethered kite is excited with zero-mean broadband white noise through the control inputs $u_{\mathrm{p}}(k)$ and $u_{\mathrm{r}}(k)$, and the resulting input-output data is used to estimate the first 500 Markov parameters.

The pitching-moment-to-pitch-angle Markov parameters suggest that $G_{\mathrm{p}}(\mathbf{z})$ has a nonminimum-phase zero near -1. Thus, the polynomial $\beta_{\mathrm{u,p}}(\mathbf{q})$ is estimated as $\beta_{\mathrm{u,p}}(\mathbf{q}) = H_{\mathrm{p},1}(\mathbf{q}+1) = 0.0013(\mathbf{q}+1)$. Similarly, the rolling-moment-to-roll-angle Markov parameters suggest that the rolling-moment-to-roll-angle transfer function has a nonminimum-phase zero near -1. Thus, we let $\beta_{\mathrm{u,r}}(\mathbf{q}) = 0.0013(\mathbf{q}+1)$.

V. Simulation Results

In this section, we present numerical examples to demonstrate control of the GTE system using RCAC. For all examples, we initialize the controllers to zero, that is, $\theta_{\mathrm{r}}(0) =$

$\theta_{\rm p}(0) = 0$, and controller orders are $n_{\rm c,r} = n_{\rm c,p} = 28$. Additionally, $\lambda_{\rm r} = \lambda_{\rm p} = 1$, $P_{\rm r}(0) = P_{\rm p}(0) = 10^{11} I_{56}$, and, as discussed above, $\beta_{\rm u,r} = \beta_{\rm u,p} = 0.0013(\mathbf{q} + 1)$.

For all examples, the GTE system has $M = 100$ kg, $\rho = 0.01 \text{kg/m}^2$, $J_1 = 833.33 \text{kg} \cdot \text{m}^2$, $J_2 = 133.33 \text{kg} \cdot \text{m}^2$, and $J_3 = 966.67 \text{kg} \cdot \text{m}^2$. Additionally, the kite has wing area 10m^2, wing span 5m, aspect ratio 2.5, wing mean chord length 2m, wing airfoil lift curve slope 2π, Glauert coefficient 0.1, Oswald efficiency factor 0.9, parasitic drag coefficient 0.05, and wing angle of zero lift $-5°$. Next, we let the slope of rolling moment coefficient versus roll angle be $-0.1/\text{rad}$ and the slope of pitching moment coefficient versus angle of attack be $-0.05/\text{rad}$. Finally, we let $q_1(0) = 400$ m, $q_2(0) = 10°$, $q_3(0) = 192°$, $q_4(0) = 2°$, $q_5(0) = 5°$, $q_6(0) = 0°$, $\dot{q}_1(0) = 5$ m/s, $\dot{q}_2(0) = 3°$/s, $\dot{q}_3(0) = -2°$/s, $\dot{q}_4(0) = 2°$/s, $\dot{q}_5(0) = 3°$/s, and $\dot{q}_6(0) = 0°$/s.

The wind velocity in the inertial x-direction is given by $10(z_{\rm alt}/30)^{1/7}$ m/s, where $z_{\rm alt}$ is the kite altitude in meters. The wind velocities in the inertial y-direction and inertial z-direction are zero. Instantaneous power equals the tension in the tether times the velocity of the tether $\dot{q}_1$.

A. Pitch Angle Command Following

In this example, we use only one RCAC control loop, specifically, we use the pitching-moment-to-pitch-angle control loop and let the rolling moment $u_{\rm r}(k)$ be identically zero. We let the external command signal (given in degrees) be $r_{\rm p}(k) = 5 + 2\sin(0.2\pi T_{\rm s} k)$. The ground-tethered kite is allowed to move open loop for 8 seconds and at 8 seconds, the adaptive controller is turned on. Figure 4 shows the ground-tethered kite's pitch angle and the command signal $r_{\rm p}$. Within several seconds of turning on the controller, the pitch angle tends toward the command signal $r_{\rm p}$. Figure 5 shows the configuration variables q_1 through q_6, and Figure 6 shows the ground-tethered kite's altitude as well as the power generated. In the 100 second simulation, the average power generated is 1.30 kW.

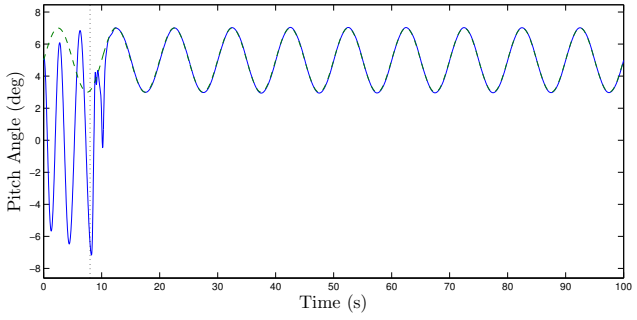

Fig. 4. *Pitch Angle Command Following:* The controller is turned on at 8 seconds, and the kite's pitch angle (solid) asymptotically tracks the command signal (dashed).

B. Pitch and Roll Angle Command Following

In this example, we use both RCAC control loops (as shown in Figure 3). The command signals (given in degrees) are $r_{\rm r}(k) = 15\sin(0.1\pi T_{\rm s} k)$ and $r_{\rm p}(k) = 5 + 2\sin(0.2\pi T_{\rm s} k)$. The GTE system initially moves open loop and at 8 seconds, both adaptive controllers are turned on. Figure 7 shows the ground-tethered kite's pitch and roll angles and the commands $r_{\rm p}$ and $r_{\rm r}$. After the controllers are turned on, the pitch and roll angles tend toward the commands $r_{\rm p}$ and $r_{\rm r}$, respectively. Figure 8 shows the variables q_1 through q_6, and Figure 9 shows the ground-tethered kite's altitude and the power generated. In the 100 second simulation, the average power generated is 1.59 kW.

The two examples given in this section demonstrate that RCAC can be used to force the kite's pitch and roll angles to follow sinusoidal command signals. Due to space considerations, plots for other command signals have been omitted. However, the adaptive controller yields similar results with a wide range of command signals, including sinusoid commands with different amplitudes and frequencies; sum-of-sinusoid command signals; and step command signals. For sum-of-sinusoid commands, the controller order should be increased to provide enough degrees of freedom for the adaptive controller to achieve internal models at each

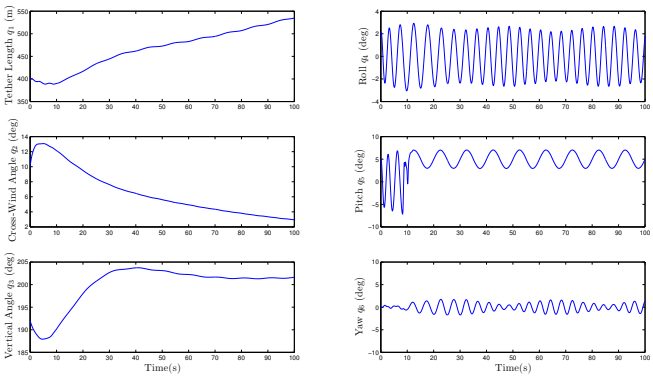

Fig. 5. *Configuration Coordinates for Pitch Angle Command Following:* The configuration variables q_1, q_2, q_3, q_4, q_5, and q_6 are well behaved with RCAC in feedback.

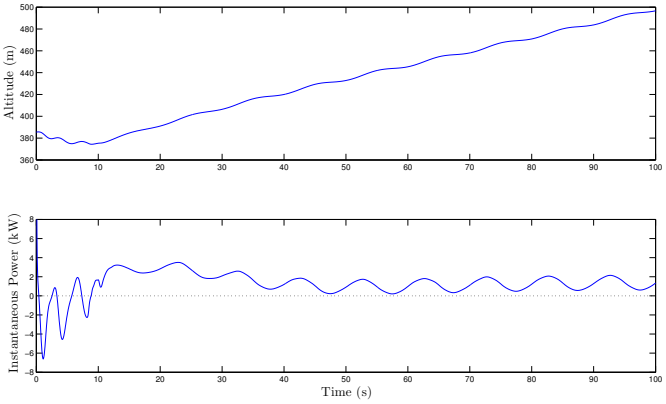

Fig. 6. *Kite Altitude and Power Generated for Pitch Angle Command Following:* The kite's altitude increases over time, and the system generates 1.30 kW of power (on average).

command frequency (see [12] for additional details).

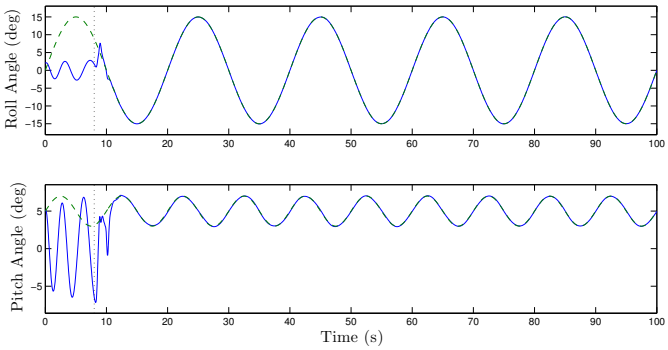

Fig. 7. *Pitch and Roll Angle Command Following:* The controller is turned on at 8 seconds, and the kite's pitch angle (solid) asymptotically tracks the command signal (dashed) while the kite's roll angle (solid) asymptotically tracks the command signal (dashed).

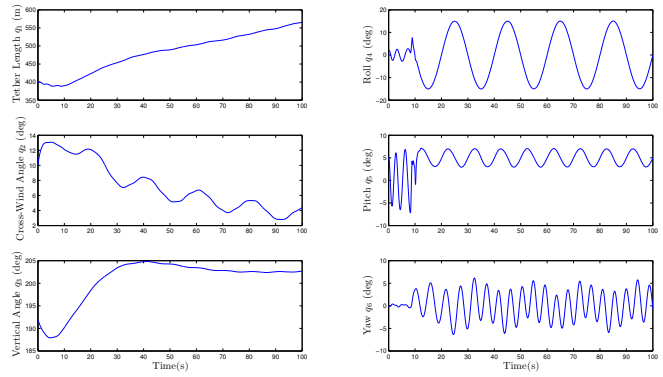

Fig. 8. *Configuration Coordinates for Pitch and Roll Angle Command Following:* The configuration variables q_1, q_2, q_3, q_4, q_5, and q_6 are well behaved with RCAC in feedback.

VI. Conclusion

In this paper, we derived the Lagrangian equations of motion for a GTE system, reviewed RCAC, and implemented RCAC on the GTE system. In particular, we demonstrated that the adaptive controller is capable of forcing the kite's pitch and roll angles to follow sinusoidal commands. Furthermore, these command trajectories resulted in positive power generation. In future work, we will explore determining the maximum-power-generating kite trajectories and following these trajectories using RCAC. In addition, future work includes extending the results of this paper to the case with time-varying wind, as well as exploring controlling the full tether extension and retraction cycle (as current simulations focus on the tether extension, or power generation phase).

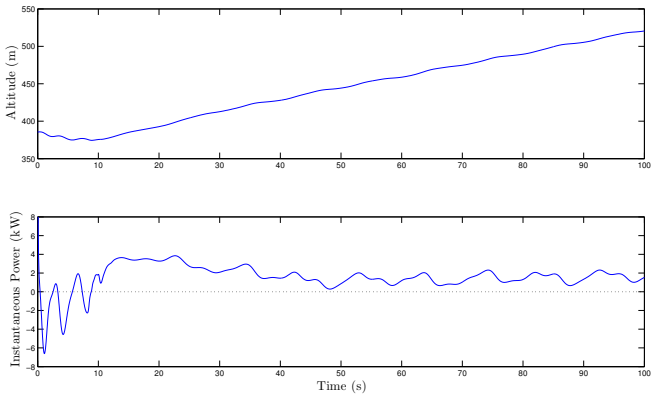

Fig. 9. *Kite Altitude and Power Generated for Pitch and Roll Angle Command Following:* The kite's altitude increases over time, and the system generates 1.59 kW of power (on average).

References

[1] "20% wind energy by 2030: Increasing wind energys contribution to U.S. electricity supply," US Department of Energy, Report DOE/GO-102008-2567, 2008.

[2] M. Canale, L. Fagiano, and M. Milanese, "Kitegen: A revolution in wind energy generation," *Energy*, vol. 34, pp. 355–361, 2009.

[3] M. L. Loyd, "Crosswind kite power," *Energy*, vol. 4, no. 3, pp. 106–111, 2006.

[4] C. A. J. Fletcher, A. J. Honan, and J. S. Sappupo, "Aerodynamic platform comparison for jet stream electricity generation," *Energy*, vol. 7, pp. 17–24, 1983.

[5] J. S. Goela, R. Vijaykumar, and R. H. Zimmermann, "Performance characteristics of a kite-powered pump," *J. Energy Resource Tech.*, vol. 108, pp. 188–193, 1986.

[6] P. Williams, B. Lansdorp, and W. Ockels, "Optimal crosswind towing and power generation with tethered kites," *Journal of Guidance, Control and Dynamics*, vol. 31, no. 1, pp. 81–93, 2008.

[7] ——, "Nonlinear control and estimation of a tethered kite in changing wind conditions," *Journal of Guidance, Control and Dynamics*, vol. 31, no. 3, pp. 793–798, 2008.

[8] I. Aragatov, P. Rautakorpi, and R. Silvenoinen, "Estimation of the mechanical energy output of the kite wind generator," *Renewable Energy*, vol. 34, pp. 1525–1532, 2009.

[9] D. J. Olinger and J. S. Goela, "Performance characteristics of a 1 kw scale kite-powered system," *ASME Journal of Solar Energy Engineering*, vol. 132, no. 4, pp. 1–11, 2010.

[10] A. Ilzhofer, B. Houska, and M. Diehl, "Nonlinear mpc of kites under varying wind conditions for a new class of large-scale wind power generators," *International Journal of Robust and Nonlinear Control*, vol. 17, pp. 1590–1599, 2006.

[11] J. B. Hoagg and D. S. Bernstein, "Cumulative retrospective cost adaptive control with RLS-based optimization," in *Proc. Amer. Contr. Conf.*, Baltimore, MD, June 2010, pp. 4016–4021.

[12] ——, "Retrospective cost adaptive control for nonminimum-phase discrete-time systems, Part 1 and Part 2," in *Proc. Conf. Dec. Contr.*, Atlanta, GA, December 2010, pp. 893–904.

[13] R. Venugopal and D. S. Bernstein, "Adaptive disturbance rejection using ARMARKOV/Toeplitz models," *IEEE Trans. Contr. Sys. Tech.*, vol. 8, pp. 257–269, 2000.

[14] M. A. Santillo and D. S. Bernstein, "Adaptive control based on retrospective cost optimization," *AIAA J. Guid. Contr. Dyn.*, vol. 33, pp. 289–304, 2010.

[15] R. C. Nelson, *Flight Stability and Automatic Control*, 2nd ed. McGraw Hill, 1998.

[16] J. Roskam, *Airplane Flight Dynamics and Automatic Flight Control*. DARcorporation, 2001.

[17] B. Etkin and L. D. Reid, *Dynamics of Flight: Stability and Control*. John Wiley and Sons, Inc., 1995.

[18] J. N. Juang, *Applied System Identification*. Upper Saddle River, NJ: Prentice-Hall, 1993.